

---

## MAJOR PAPER

---

# Low WSS and High OSI Measured by 3D Cine PC MRI Reflect High Pulmonary Artery Pressures in Suspected Secondary Pulmonary Arterial Hypertension

Masaki TERADA<sup>1</sup>, Yasuo TAKEHARA<sup>2\*</sup>, Haruo ISODA<sup>3</sup>, Tomohiro UTO<sup>4</sup>,  
Masaki MATSUNAGA<sup>5</sup>, and Marcus ALLEY<sup>6</sup>

<sup>1</sup>*Department of Diagnostic Radiological Technology, Iwata City Hospital,  
512-3 Okubo, Iwata, Shizuoka, 438-8550 Japan*

<sup>2</sup>*Department of Radiology, Hamamatsu University Hospital*

<sup>3</sup>*Brain & Mind Research Center, Nagoya University*

<sup>4</sup>*Department of Respiratory Medicine, Iwata City Hospital*

<sup>5</sup>*Department of Cardiology, Iwata City Hospital*

<sup>6</sup>*Department of Radiology, Stanford University School of Medicine*

(Received April 13, 2015; Accepted September 14, 2015; published online November 13, 2015)

**Purpose:** Institutional Review Board (IRB)-approved prospective study was conducted to test whether objective and quantitative hemodynamic markers wall shear stress (WSS) and oscillatory shear index (OSI) measured by three-dimensional (3D) cine phase-contrast (PC) can reflect pulmonary arterial hypertension (PAH).

**Patients and Methods:** Seventeen consecutive patients of suspected secondary PAH were examined for pulmonary artery pressures (PAPs) with right heart catheterization (RHC) and three-dimensional (3D) cine PC MR. Based on the RHC data, patients were subdivided into two groups of 12 non-PAH (median age of 74.5 years) and 5 PAH (median age of 77 years) patients. Based on 3D cine PC magnetic resonance (MR), hemodynamic parameters including spatially averaged systolic WSS (sWSS), diastolic WSS (dWSS), mean WSS (mWSS), OSI and blood vessel section area (BVSA) at the pulmonary arterial trunk were calculated. Streamline images in the pulmonary arteries were also assessed. All the parameters were compared between non-PAH and PAH groups.

**Results:** sWSS (N/m<sup>2</sup>) and mWSS (N/m<sup>2</sup>) of PAH group was lower than that of non-PAH group (0.594 ± 0.067 vs. 0.961 ± 0.590,  $P = 0.001$ ), (0.365 ± 0.035 vs. 0.489 ± 0.132,  $P = 0.027$ ). OSI of PAH group was higher than that of non-PAH (0.214 ± 0.026 vs. 0.130 ± 0.046,  $P = 0.001$ ). sWSS, mWSS, and dWSS were inversely correlated and OSI was positively correlated to mean PAP or systolic PAP with  $r$  values of  $-0.638$  ( $P = 0.005$ ),  $-0.643$  ( $P = 0.005$ ),  $-0.485$  ( $P = 0.049$ ), and  $0.625$  ( $P = 0.007$ ); or  $-0.622$  ( $P = 0.008$ ),  $-0.629$  ( $P = 0.007$ ),  $-0.484$  ( $P = 0.049$ ), and  $0.594$  ( $P = 0.012$ ), respectively. sWSS was also inversely correlated to BVSA with  $r$  value of  $-0.488$  ( $P = 0.049$ ), and OSI was correlated to BVSA with  $r$  value of  $0.574$  ( $P = 0.016$ ). Vortex or helical flows were observed more frequently in PAH patients.

**Conclusions:** The low sWSS and mWSS as well as high OSI measured with 3D cine PC MR could be potential hemodynamic markers for the increased PAP in suspected secondary PAH patients.

**Keywords:** *pulmonary arterial hypertension, three-dimensional cine phase contrast MR imaging, pulmonary arterial velocities, wall shear stress, oscillatory shear index*

---

\*Corresponding author, Phone: +81-53-435-2242, Fax: +81-53-435-2241, E-mail: takehara@hama-med.ac.jp

## Introduction

With the advancement of the clinical stages of respiratory diseases, such as chronic obstructive pulmonary disease (COPD) and interstitial pneumonia (IP), dyspnea on effort intensifies and patient activity of daily life is deteriorated. The onset of secondary pulmonary arterial hypertension (PAH), in addition to respiratory insufficiency, is thought to aggravate symptoms.<sup>1-3</sup> Therefore, respiratory and cardiovascular physicians have been increasingly focused on the evaluation of PAH in the management of the patients with respiratory diseases.

PAH, characterized by peripheral blood vessel contraction and vascular remodeling, is a pulmonary vascular disease that leads to a gradual increase in pulmonary vascular resistance. The current standard diagnostic technique that is routinely employed to evaluate hemodynamics of PAH patients is right heart catheterization (RHC).<sup>4-6</sup> Due to the relative invasiveness of RHC, alternative non-invasive methods have been sought for the analysis of hemodynamics.<sup>7-13</sup> For this purpose, hemodynamic information derived from flowmetry with two-dimensional (2D) phase contrast (PC) magnetic resonance (MR) technique such as acceleration time (AT)<sup>7</sup> or peak velocity (PV)<sup>7,8</sup> have been tested for potential indicators of PAH (Fig. 1). However, the 2DFT method sometimes suffers from inconsistent data depending on the prescribed measurement planes in the pulmonary arteries. Most profound weakness of the 2D PC cine MR is that the measurement planes cannot be optimized during the examination. With phase-resolved 3D PC images, more robust, quantitative, visual recognitions of the flow dynamics of the whole pulmonary arteries are allowed. Once data are acquired, retrospective measurements of hemodynamic parameters are available.

In this study, we have investigated whether hemodynamic parameters of the 3D MR flowmetry such as wall shear stress (WSS)<sup>14-17</sup> or oscillatory shear index (OSI) can reflect PAH.

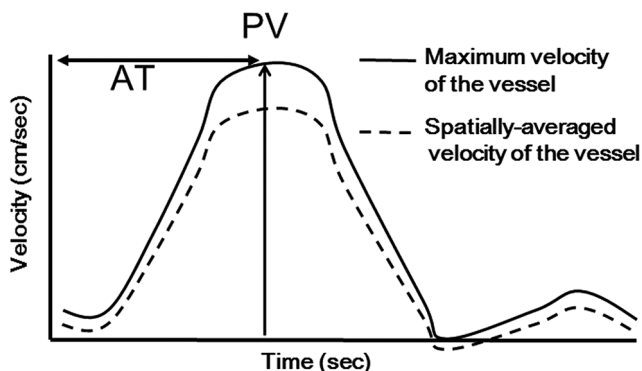


**Fig. 1.** The definitions of acceleration time (AT) and peak velocity (PV).

## Materials and Methods

Institutional Review Board (IRB) approved the prospective study which was conducted between April 2011 and December 2013.

### Patients

Seventeen consecutive patients with respiratory diseases who were suspected of having PAH by routine cardiac ultrasonography were enrolled in the study. Written informed consent was obtained from all patients. All patients underwent RHC and 3D cine PC MR. The subjects comprised 14 males and 3 females with mean age of 75.2 years. Based on the RHC data, 5 patients were diagnosed as PAH (3 males, 2 females, median age of 77 years) and 12 patients were diagnosed as non-PAH (11 males, 1 females, median age of 74.5 years). Patient demographics are shown in Table 1.

### MR system and imaging parameters

All patients underwent 3D cine PC MR on a 3T MR system (Signa HDxt, General Electric Healthcare, Waukesha, Wisconsin, USA) with a 32-channel cardiac phased array coil.

With 3D cine PC MR, 3D volume data of magnitude images and phase images with velocity components over time were obtained.<sup>15-17</sup> Oblique-axial sections covering the whole pulmonary artery trunk and right and left main pulmonary arteries were prescribed. Electrocardiogram (ECG) gating and respiratory compensation were also combined.<sup>17</sup> The parameters for 3D cine PC MR were: repetition time (TR)/echo time (TE)/flip angle (FA)/number of excitations (NEXs) of 5.6/2.8/9/1; field of view (FOV) of  $350 \times 260 \times 60$  mm; matrix of  $256 \times 224 \times 30$  [ $256 \times 224 \times 60$  with zero filled interpolation (ZIP)]; voxel size of  $1.3 \times 1.2 \times 2$  mm<sup>3</sup> ( $1.3 \times 1.3 \times 1$  mm<sup>3</sup> with ZIP); receiver bandwidth of 62.5 kHz/FOV; 20 phases/cardiac cycle; velocity encoding (VENC) of 150 cm/s; view per segment (VPS) of 4; in plane reduction factor for autocalibrating reconstruction for Cartesian imaging (ARC) of 2. Scan time was 8.2 min on average. To avoid an aliasing in velocimetry, relatively high VENC of 150 cm/s was adopted.

### Data processing

Magnitude images of 3D cine PC MR and phase images of each three orthogonal directions were transferred to a personal computer (2.1-GHz Intel Core i3 CPU, Microsoft Windows 7 in DICOM format. MR image data were post-processed with flow analysis software (Flova, R<sup>2</sup>Tech Co. Ltd., Hamamatsu, Shizuoka).

Pulmonary arterial boundary was segmented based on the intensities of both magnitude images and phase images obtained with 3D cine PC MR.<sup>18</sup> Segmentation was done by region growing method, and then morphological boundary was determined by the marching cube method.

**Table 1.** Patients' demographics of non-PAH subgroups and PAH subgroups

non-PAH			PAH		
n = 12			n = 5		
Sex (M/F)		11/1	Sex (M/F)		3/2
Age (median, range)		74.5 (57–83)	Age (median, range)		77 (73–88)
Diagnosis	CVD-IP	2	Diagnosis	IIP	1
	IIP	1		PAH	1
	COPD	4		COPD	2
	IP+COPD	3		Postoperation of lung cancer	1
	Sarcoidosis	1			
	NTM	1			
BNP (pg/ml)		78.4 ± 52.2*	BNP (pg/ml)		174.7 ± 186*
A-aDO <sub>2</sub> (mmHg)		46.9 ± 20.7	A-aDO <sub>2</sub> (mmHg)		35.3 ± 21.6
sPAP(UCG, mmHg)		50.8 ± 19.3	sPAP (UCG, mmHg)		52.6 ± 16.6
mPAP (RHC, mmHg)		18.3 ± 3.7*	mPAP (RHC, mmHg)		33.6 ± 7.0*
Data are presented as mean ± SD.			*:statistically significant ( <i>P</i> values < 0.05).		

A-aDO<sub>2</sub>, alveolar-arterial oxygen difference; BNP, brain natriuretic peptide; COPD, chronic obstructive pulmonary disease; CVD-IP, collagen vascular disease-interstitial pneumonia; F, female; IIP, idiopathic interstitial pneumonia; IP, interstitial pneumonia; M, male; NTM, nontuberculous mycobacteriosis; sPAP, systolic pulmonary arterial pressure; mPAP, mean pulmonary arterial pressure; PAH, pulmonary arterial hypertension; RHC, right heart catheterization; SD, standard deviation; UCG, ultrasound cardiography.

Velocity data in each voxel included inside the vascular boundary were incorporated from phase images with resolution of 1.5 mm and a time-course 3D velocity field containing a time component was obtained.

#### Measurements of the conventional hemodynamic markers

Hemodynamic parameters AT and PV were analyzed on the cross section perpendicular to the pulmonary artery trunk 1 cm proximal to the bifurcation. Blood vessel section area (BVSA) was also measured at the same location. AT was defined as the time from the beginning of antegrade flow to the systolic flow peak.<sup>7</sup> PV was defined as the peak speed of the systolic blood flow (Fig. 1).

#### Measurements of WSS and OSI

WSS is a dynamic frictional force induced by blood flow along the surface of the vascular walls.<sup>19–21</sup> OSI was defined as “fluctuation” of the WSSs of the vascular wall.<sup>22</sup> Two independent operators (M.T. and K.M) with 9-year and 7-year experiences in flow analysis measured systolic WSS (sWSS), diastolic WSS (dWSS), and mean WSS (mWSS) by placing cylindrical ROI (width of 3 pixels and the mean size of the ROI was 208 pixels) surrounding the pulmonary artery trunk at 1 cm proximal to the bifurcation.

#### Streamline analysis

Streamline images<sup>14,15,22,23</sup> within the pulmonary artery were delineated for each patient with the flow

analysis software. Abnormal hemodynamic patterns such as vortex or helical flow patterns were blindly assessed by two independent observers (Y.T. and M.T.) with 9 years experience in flow analysis. The degree of abnormal flow patterns were rated in three grades as 0 (none, consistent laminar flow without any discernible vortex or helical flow): 1 (moderate, one abnormal flow pattern involving more than 1/3 area of the lumen of the pulmonary trunk): 2 (severe, more than two abnormal flow patterns involving more than 1/3 of the lumen of the pulmonary trunk). The rating was performed separately for systole and diastole. The abnormal flow patterns could be instantaneous or prolonged during the period of observations.

#### Statistics

AT, PV, sWSS, dWSS, mWSS, OSI, and BVSA obtained by MR were compared between non-PAH and PAH groups with non-parametric Mann-Whitney U test with Bonferroni's correction.

Regression analysis was performed to test whether PAP measured by RHC correlated with hemodynamic parameters AT, PV, sWSS, dWSS, mWSS, OSI, and BVSA. Intra and interoperator agreement concerning the measurements of sWSS, dWSS, mWSS, and OSI by two operators were also assessed by regression analysis as well as Bland-Altman analysis. The regressions were examined by Spearman's rank correlation coefficient. A *P* value less than 0.05 was considered statistically significant.

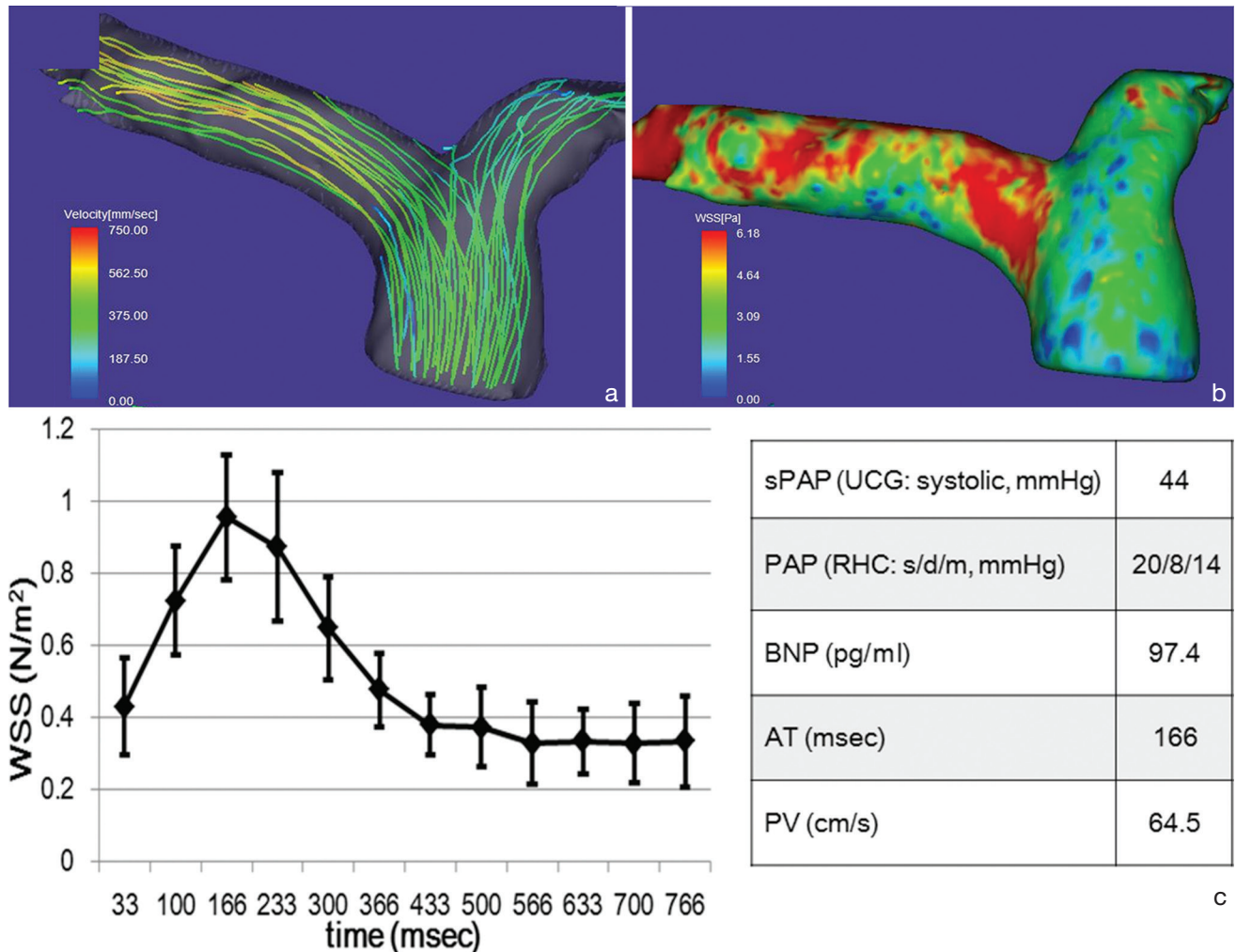


**Fig. 2.** Representative streamline analysis (a), WSS map (b), time course changes of the WSS values of the main pulmonary arterial wall and hemodynamic values (c) acquired in a 77-year-old male with non-PAH. Systolic streamlines of the pulmonary artery (a) show laminar, but no vortex flow. WSS in the time-averaged WSS-contour image of the pulmonary artery (b) is about 3 N/m<sup>2</sup> or more. Spatially-averaged temporal WSS change in the pulmonary artery (c) show its peak at 166 ms from R wave (systole). Patients’ data with non-PAH demonstrates a high value of BNP and normal PAP. The error bars represent the SD. AT, acceleration time; BNP, brain natriuretic peptide; PAH, pulmonary arterial hypertension; PAP, pulmonary arterial pressure; PV, peak velocity; RHC, right heart catheterization; s/d/m, systole/diastole/mean; sPAP, systolic pulmonary arterial pressure; UCG, ultrasound cardiography; WSS, wall shear stress.

Streamlines of pulmonary arteries were compared between the PAH and non-PAH patients. Interobserver variabilities concerning the abnormal flow patterns within the pulmonary arteries were analyzed by kappa statistics. Kappa values below 0.2 were interpreted as poor, 0.21–0.40 as fair, 0.41–0.60 as moderate, 0.61–0.8 as good, and 0.81–1.0 as very good agreements.

**Results**

The results of hemodynamic data obtained by 3D cine PC MR are compared between the PAH and non-PAH patients (Figs. 2a–c, 3a–c; Table 2). sWSS, mWSS, OSI, and BVSA at the pulmonary artery trunk was significantly different between the PAH and non-PAH patients. sWSS (N/m<sup>2</sup>) and mWSS (N/m<sup>2</sup>) of PAH group were lower

than those of non-PAH group; ( $0.594 \pm 0.067$  vs.  $0.961 \pm 0.590$ ,  $P = 0.001$ ) and ( $0.365 \pm 0.035$  vs.  $0.489 \pm 0.132$ ,  $P = 0.027$ ). OSI of PAH group was higher than that of non-PAH group; ( $0.214 \pm 0.026$  vs.  $0.130 \pm 0.046$ ,  $P = 0.001$ ). BVSA of PAH group was larger than that of non-PAH group; ( $1104.5 \pm 62.1$  vs.  $684.1 \pm 129.1$ ,  $P = 0.009$ ).

The results comparing between hemodynamic data obtained by 3D cine PC MR and PAP are shown in Table 3. OSI and BVSA had a significantly positive correlation with mPAP, sPAP, and dPAP. PV, sWSS, dWSS, and mWSS had a negative correlation with mPAP and sPAP. Particularly, sWSS ( $r = -0.638$ ,  $P = 0.005$ ) and mWSS ( $r = -0.643$ ,  $P = 0.005$ ) had an obvious negative correlation with mPAP above all.

The results comparing between hemodynamic data obtained by 3D cine PC MR and BVSA are shown in

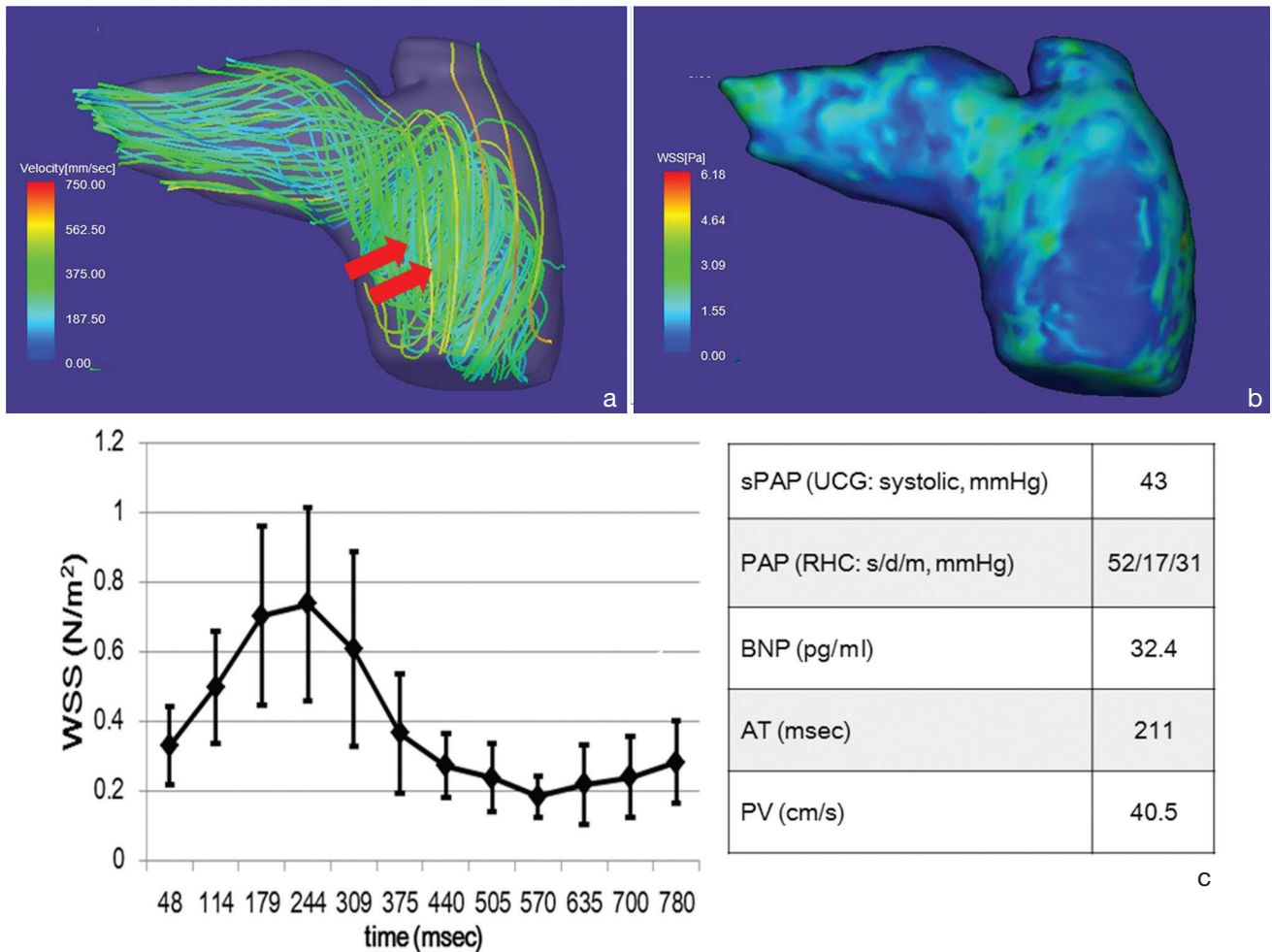


**Fig. 3.** Representative streamline analysis (a), WSS map (b), time course changes of the WSS values of the main pulmonary arterial wall and hemodynamic values (c) acquired in a 75-year-old female with PAH. Streamlines of the pulmonary artery (a) show vortex flow (arrows) from the trunk to right pulmonary artery. WSS in the time-averaged WSS-contour image of the pulmonary artery (b) is about 1.5 N/m<sup>2</sup> or less. Spatially-averaged temporal WSS changes in the pulmonary artery (c) show its peak at systole (244 ms from R wave), which is lower than non-PAH (Fig. 2c). The error bars represent the standard deviation. Patient’s data with PAH demonstrates that PAP is higher, BNP is lower, AT is higher and PA is lower as compared with non PAH patients. AT, acceleration time; BNP, brain natriuretic peptide; PAH, pulmonary arterial hypertension; PAP, pulmonary arterial pressure; PV, peak velocity; RHC, right heart catheterization; s/d/m, systole/diastole/mean; sPAP, systolic pulmonary arterial pressure; UCG, ultrasound cardiography; WSS, wall shear stress.

**Table 2.** Differences of pulmonary arterial hemodynamic parameters between patients with and without pulmonary hypertension based on 3D cine phase contrast MR imaging data

	Total	Patients with PAH	Patients without PAH	P value
No. of patients	17	5	12	–
AT (msec)	0.189 ± 0.026	0.185 ± 0.020	0.192 ± 0.027	0.855
PV (cm/sec)	53.02 ± 10.34	47.82 ± 8.33	55.19 ± 10.63	0.328
sWSS (N/m <sup>2</sup> )	0.853 ± 0.257	0.594 ± 0.067	0.961 ± 0.590	0.001
dWSS (N/m <sup>2</sup> )	0.257 ± 0.068	0.216 ± 0.072	0.275 ± 0.062	0.13
mWSS (N/m <sup>2</sup> )	0.453 ± 0.125	0.365 ± 0.035	0.489 ± 0.132	0.027
OSI	0.155 ± 0.056	0.214 ± 0.026	0.130 ± 0.046	0.001
BVSA (mm <sup>2</sup> )	807.7 ± 226.8	1104.5 ± 62.1	684.1 ± 129.1	0.009

AT, acceleration time; BVSA, blood vessel section area; dWSS, diastolic wall shear stress; mWSS, mean wall shear stress; OSI, oscillatory shear index; PAH, pulmonary arterial hypertension; PV, peak velocity; sWSS, systolic wall shear stress.

**Table 3.** Correlation coefficients between pulmonary artery hemodynamic parameters based on three-dimensional cine phase contrast magnetic resonance and pulmonary pressures based on right heart catheterization

Parameter	mPAP	sPAP	dPAP
AT	-0.170 ( $P = 0.514$ )	-0.115 ( $P = 0.661$ )	-0.246 ( $P = 0.342$ )
PV	-0.498 ( $P = 0.044$ )	-0.482 ( $P = 0.049$ )	-0.274 ( $P = 0.287$ )
sWSS	-0.638 ( $P = 0.005$ )	-0.622 ( $P = 0.008$ )	-0.426 ( $P = 0.088$ )
dWSS	-0.485 ( $P = 0.049$ )	-0.484 ( $P = 0.049$ )	-0.108 ( $P = 0.681$ )
mWSS	-0.643 ( $P = 0.005$ )	-0.629 ( $P = 0.007$ )	-0.408 ( $P = 0.104$ )
OSI	0.625 ( $P = 0.007$ )	0.594 ( $P = 0.012$ )	0.647 ( $P = 0.005$ )
BVSA	0.523 ( $P = 0.031$ )	0.515 ( $P = 0.034$ )	0.659 ( $P = 0.004$ )

AT, acceleration time; BVSA, blood vessel section area; dWSS, diastolic wall shear stress; mWSS, mean wall shear stress; OSI, oscillatory shear index; PAH, pulmonary arterial hypertension; PV, peak velocity; sWSS, systolic wall shear stress.

**Table 4.** Correlation coefficients between pulmonary artery hemodynamic parameters and pulmonary trunk blood vessel section area based on three-dimensional cine phase contrast magnetic resonance

Parameter	BVSA
AT	-0.174 ( $P = 0.567$ )
PV	-0.192 ( $P = 0.525$ )
sWSS	-0.488 ( $P = 0.049$ )
dWSS	-0.105 ( $P = 0.687$ )
mWSS	-0.306 ( $P = 0.232$ )
OSI	0.574 ( $P = 0.016$ )

AT, acceleration time; BVSA, blood vessel section area; dWSS, diastolic wall shear stress; mWSS, mean wall shear stress; OSI, oscillatory shear index; PV, peak velocity; sWSS, systolic wall shear stress.

Table 4. WSS and OSI were related to the size of the cross-sectional area of the pulmonary trunk. sWSS ( $r = -0.488$ ,  $P = 0.049$ ) had a negative correlation with BVSA, and OSI on the other hand, had a positive correlation with BVSA ( $r = 0.574$ ,  $P = 0.016$ ).

There were acceptable to negligible variability between two observers concerning the appearances of the abnormal flow patterns with kappa values of 0.545 (moderate agreement) to 0.750 (substantial agreement). The assessments of the pulmonary streamlines performed by the two observers are shown in Table 5. Severe abnormal flow patterns (grade 2) were observed in 1 to 2 out of 5 PAH patients during systole and diastole, and none in non-PAH patients (Figs. 2a, 3a). Mild abnormal flow patterns (grade 1) were observed in 2 to 3 during systole and 3 to 4 during diastole out of 5 PAH patients, and in 2 during systole and 9 to 10 during diastole out of 12 non-PAH patients.

The intraoperator coefficients for all parameters (sWSS, dWSS, mWSS and OSI) were good (0.897 to 0.973) while those of the interoperator were excellent (0.939 to 0.980) (Table 6). Bland-Altman plots were also within the acceptable ranges of the bias (Fig. 4a-i).

## Discussion

Previously, limited hemodynamic parameters such as AT or PV have been reported to be indicators for PAH.<sup>7,8</sup> In this study, WSS and OSI were assessed as potential indicators of secondary PAH, and they better reflected the PAP than conventional markers such as AT or PV. WSS is an instantaneous measure of the velocity gradient near the arterial wall. OSI is a temporal change of WSS as a function of the cardiac phases. We deem both WSS and OSI are essential in analyzing the abnormalities of the flow dynamics, because low WSS at single time point alone cannot precisely indicate the temporal abnormalities of the flow dynamics.

When sWSS and mWSS were compared between PAH and non-PAH patients, they were also significantly lower in the PAH patients, and sWSS and mWSS showed inverse linear regression with sPAP and mPAP. As the causative factors, it was hypothesized that the systolic and mean flow velocity was decreased by helical or vortex flow due to the high PAP. In an analysis of pulmonary embolism patients, Sanz et al.<sup>7</sup> have reported that the peak velocity and average velocity of the blood flow within the pulmonary arteries had moderate to high inverse correlations to mPAP. In a sub-group of PAH, there was a weak correlation between peak velocity and mPAP.<sup>7</sup> In addition, our results showed that BVSA and PAP at the pulmonary artery trunk had a positive linear correlation. Increased BVSA in PAP reflects positive remodeling of the pulmonary artery. It was presumed that the dilatation of the flow path resulted in a loss of

**Table 5.** The variations between two observers concerning the appearances of the abnormal flow patterns on pulmonary artery streamlines images

Cardiac phase		Systole			Diastole		
		Grade 0	Grade 1	Grade 2	Grade 0	Grade 1	Grade 2
PAH	Observer 1	1	2	2	0	4	1
	Observer 2	1	3	1	0	3	2
non-PAH	Observer 1	10	2	0	3	9	0
	Observer 2	10	2	0	2	10	0

Figures indicate the number of the patients. Grade 0: no abnormal flow (laminar flow in the systole and turbulent flow in the diastole); Grade 1, mild vortex and/or helical flow; Grade 2, severe vortex and/or helical flow; PAH, pulmonary arterial hypertension.

**Table 6.** Intraoperator and interoperator correlation coefficients for measurements of wall shear stress and oscillatory shear index

Parameter	Intraoperator 1	Intraoperator 2	Interoperator
sWSS	0.973 ( $P < 0.001$ )	0.951 ( $P < 0.001$ )	0.980 ( $P < 0.001$ )
dWSS	0.953 ( $P < 0.001$ )	0.897 ( $P < 0.001$ )	0.939 ( $P < 0.001$ )
mWSS	0.951 ( $P < 0.001$ )	0.931 ( $P < 0.001$ )	0.958 ( $P < 0.001$ )
OSI	0.941 ( $P < 0.001$ )	0.924 ( $P < 0.001$ )	0.939 ( $P < 0.001$ )

dWSS, diastolic wall shear stress; mWSS, mean wall shear stress; OSI, oscillatory shear index; sWSS, systolic wall shear stress.

blood flow momentum, which caused vortex and helical flow within the dilated pulmonary arteries.<sup>10</sup> It is also presumed that the increased pulmonary vascular resistance and decreased compliance of the pulmonary arterial wall prevent smooth antegrade laminar flow toward the lung. This may cause reflected wave from the downstream blood flow to the upstream. The collision of the antegrade and retrograde flow may cause vortex or helical flow instead of laminar. Observers in this study recognized a vortex or spiral flow patterns during systole on the streamline images in 4 out of 5 patients of PAH, which may be reflecting this phenomena.

It was also noteworthy that OSI was significantly lower in the non-PAH patients and significantly higher in the PAH patients. In addition, OSI had a positive linear correlation with PAP. OSI is a sensitive indicator of chronological fluctuations of the local WSS, and it was speculated that OSI was influenced by irregular flow, particularly regurgitation that is more common in the PAH patients.<sup>10</sup>

Related to the phenomenon stated above, previous reports suggested that nitric oxide (NO) production is decreased in the endothelial cells that cover the pulmonary arteries of the PAH patient, and the dysfunction of endothelial cells have been reported to be a factor for peripheral pulmonary arterial vasoconstrictions and further progress of PAH.<sup>24-26</sup> As a mechanoreceptor, endothelial cells are markedly sensitive to the changes of the WSS or OSI.<sup>27</sup> Decreased WSS and increased

OSI detected by vascular endothelium prohibit NO production and release atherogenic substances instead.<sup>28-32</sup> It is therefore implicated that once an abnormal flow dynamics become dominant, they aggravate stiffness of the pulmonary artery and the vasoconstrictions of the peripheral pulmonary circulations, which cause abnormal flow dynamics, and then promote this vicious cycle. 3D cine PC MR is currently the only method that allows for direct and non-invasive measurement of these hemodynamic markers *in-vivo*.

Compared with 2D cine PC MR, 3D cine PC MR allows for 3D visual recognitions of the pulmonary artery, which is helpful in determining the measurement planes. Retrospective settings of the arbitrary planes can help avoid errors in flowmetry caused by inappropriately prescribed measurement planes that was often the case with 2D cine PC. In addition, with 3DFT data acquisition, SNR of the phase images is significantly improved. Moreover, 3D maps of the WSS and OSI color-coded on the pulmonary arteries can be generated quickly, and they allow more objective visual recognitions of spatial and temporal understandings of the abnormal flow dynamics taking place in the pulmonary arteries than mere numerical values.<sup>28</sup>

The limitations of this study are the relatively small number of patient population and the low temporal resolutions of the 3D cine PC MR for the cardiac phase, which may miss subtle temporal changes of the flow dynamics.

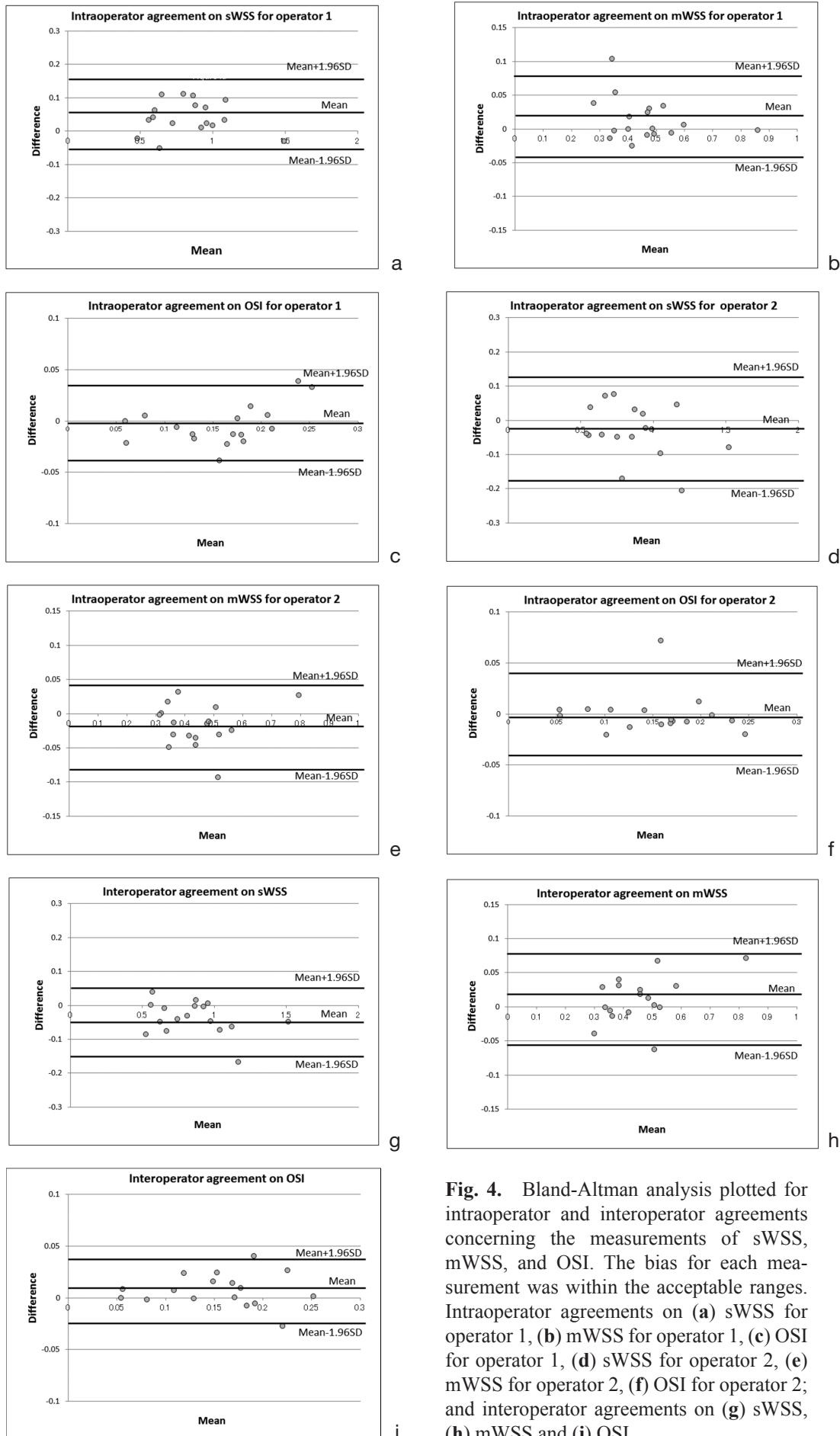


**Fig. 4.** Bland-Altman analysis plotted for intraoperator and interoperator agreements concerning the measurements of sWSS, mWSS, and OSI. The bias for each measurement was within the acceptable ranges. Intraoperator agreements on (a) sWSS for operator 1, (b) mWSS for operator 1, (c) OSI for operator 1, (d) sWSS for operator 2, (e) mWSS for operator 2, (f) OSI for operator 2; and interoperator agreements on (g) sWSS, (h) mWSS and (i) OSI.



## Conclusion

In conclusion, our study suggested that sWSS, mWSS, and OSI of the pulmonary arterial trunk measured by 3D cine PC MR could be potential hemodynamic markers for the increased PAP in suspected secondary PAH patients.

## Acknowledgments

The authors thank Masaya Hirano, Atsushi Nozaki, Tetsuya Wakayama, and Hiroyuki Kabasawa of GE Healthcare Japan and Keigo Matsuyoshi of Iwata City Hospital for their technological assistances.

## References

- Andersen CU, Mellekjær S, Nielsen-Kudsk JE, Bendstrup E, Hilberg O, Simonsen U. Pulmonary hypertension in chronic obstructive and interstitial lung diseases. *Int J Cardiol* 2013; 168:1795–1804.
- Simonneau G, Galiè N, Rubin LJ, et al. Clinical classification of pulmonary hypertension. *J Am Coll Cardiol* 2004; 43:5S–12S.
- McLaughlin VV, Presberg KW, Doyle RL, et al. Prognosis of pulmonary arterial hypertension: ACCP evidence-based clinical practice guidelines. *Chest* 2004; 126(1 Suppl):78S–92S.
- Barst RJ, McGoon M, Torbicki A, et al. Diagnosis and differential assessment of pulmonary arterial hypertension. *J Am Coll Cardiol* 2004; 43(12 Suppl S):40S–47S.
- Galiè N, Manes A, Branzi A. Evaluation of pulmonary arterial hypertension. *Curr Opin Cardiol* 2004; 19:575–581.
- Simonneau G, Robbins IM, Beghetti M, et al. Updated clinical classification of pulmonary hypertension. *J Am Coll Cardiol* 2009(1 Suppl 1); 54:S43–S54.
- Sanz J, Kuschnir P, Rius T, et al. Pulmonary arterial hypertension: noninvasive detection with phase-contrast MR imaging. *Radiology* 2007; 243:70–79.
- Ley S, Mereles D, Puderbach M, et al. Value of MR phase-contrast flow measurements for functional assessment of pulmonary arterial hypertension. *Eur Radiol* 2007; 17:1892–1897.
- Mousseaux E, Tasu JP, Jolivet O, Simonneau G, Bittoun J, Gaux JC. Pulmonary arterial resistance: noninvasive measurement with indexes of pulmonary flow estimated at velocity-encoded MR imaging—preliminary experience. *Radiology* 1999; 212:896–902.
- Bogren HG, Klipstein RH, Mohiaddin RH, et al. Pulmonary artery distensibility and blood flow patterns: a magnetic resonance study of normal subjects and of patients with pulmonary arterial hypertension. *Am Heart J* 1989; 118:990–999.
- Tardivon AA, Mousseaux E, Brenot F, et al. Quantification of hemodynamics in primary pulmonary hypertension with magnetic resonance imaging. *Am J Respir Crit Care Med* 1994; 150:1075–1080.
- Wacker CM, Schad LR, Gehling U, et al. The pulmonary artery acceleration time determined with the MR-RACE-technique: comparison to pulmonary artery mean pressure in 12 patients. *Magn Reson Imaging* 1994; 12:25–31.
- Laffon E, Vallet C, Bernard V, et al. A computed method for noninvasive MRI assessment of pulmonary arterial hypertension. *J Appl Physiol* (1985) 2004; 96:463–468.
- Lee VS, Spritzer CE, Carroll BA, et al. Flow quantification using fast cine phase-contrast MR imaging, conventional cine phase-contrast MR imaging, and Doppler sonography: in vitro and in vivo validation. *AJR Am J Roentgenol* 1997; 169:1125–1131.
- Markl M, Chan FP, Alley MT et al. Time-resolved three-dimensional phase-contrast MRI. *J Magn Reson Imaging* 2003; 17:499–506.
- Bammer R, Hope TA, Aksoy M, et al. Time-resolved 3D quantitative flow MRI of the major intracranial vessels: initial experience and comparative evaluation at 1.5T and 3.0T in combination with parallel imaging. *Magn Reson Med* 2007; 57:127–140.
- Markl M, Harloff A, Bley TA, et al. Time-resolved 3D MR velocity mapping at 3T: improved navigator-gated assessment of vascular anatomy and blood flow. *J Magn Reson Imaging* 2007; 25:824–831.
- Bock J, Frydrychowicz A, Stalder AF, et al. 4D phase contrast MRI at 3 T: effect of standard and blood-pool contrast agents on SNR, PC-MRA, and blood flow visualization. *Magn Reson Med* 2010; 63:330–338.
- Masaryk AM, Frayne R, Unal, O, Krupinski E, Strother CM. In vitro and in vivo comparison of three MR measurement methods for calculating vascular shear stress in the internal carotid artery. *AJNR Am J Neuroradiol* 1999; 20:237–245.
- Cheng CP, Parker D, Taylor CA. Quantification of wall shear stress in large blood vessels using Lagrangian interpolation functions with cine phase-contrast magnetic resonance imaging. *Ann Biomed Eng* 2002; 30:1020–1032.
- Stalder AF, Russe MF, Frydrychowicz A, Bock J, Hennig J, Markl M. Quantitative 2D and 3D phase contrast MRI: optimized analysis of blood flow and vessel wall parameters. *Magn Reson Med* 2008; 60:1218–1231.
- He X, Ku DN. Pulsatile flow in the human left coronary artery bifurcation: average conditions. *J Biomech Eng* 1996; 118:74–82.
- Dumoulin CL. Phase contrast MR angiography techniques. *Magn Reson Imaging Clin N Am* 1995; 3: 399–411.
- Peinado VI, Barbera JA, Ramirez J, et al. Endothelial dysfunction in pulmonary arteries of patients with mild COPD. *Am J Physiol* 1998; 274(6 pt 1):L908–L913.
- Barberà JA, Blanco I. Pulmonary hypertension in patients with chronic obstructive pulmonary disease: advances in pathophysiology and management. *Drugs* 2009; 69:1153–1171.
- Giaid A, Michel RP, Stewart DJ, Sheppard M, Corrin B, Hamid Q. Expression of endothelin-1 in lungs of patients with cryptogenic fibrosing alveolitis. *Lancet* 1993; 341:1550–1554.

27. Malek AM, Alper SL, Izumo S. Hemodynamic shear stress and its role in atherosclerosis. *JAMA* 1999; 282:2035–2042.
  28. Barker AJ, Roldán-Alzate A, Entezari P, et al. Four-dimensional flow assessment of pulmonary artery flow and wall shear stress in adult pulmonary arterial hypertension: results from two institutions. *Magn Reson Med* 2015; 73:1904–1913.
  29. Malek AM, Izumo S, Alper SL. Modulation by pathophysiological stimuli of the shear stress-induced up-regulation of endothelial nitric oxide synthase expression in endothelial cells. *Neurosurgery* 1999; 45: 334–344; discussion 344–335.
  30. Malek AM, Jiang L, Lee I, Sessa WC, Izumo S, Alper SL. Induction of nitric oxide synthase mRNA by shear stress requires intracellular calcium and G-protein signals and is modulated by PI 3 kinase. *Biochem Biophys Res Commun* 1999; 254:231–242.
  31. Gimbrone MA Jr, Resnick N, Nagel T, Khachigian LM, Collins T, Topper JN: Hemodynamics, endothelial gene expression, and atherogenesis. *Ann N Y Acad Sci* 1997; 811: 1–11; discussion 10–1.
  32. Nishida K, Harrison DG, Navas JP, et al. Molecular cloning and characterization of the constitutive bovine aortic endothelial cell nitric oxide synthase. *J Clin Invest* 1992; 90: 2092–2096.
-